

SAMix: Calibrated and Accurate Continual Learning via Sphere-Adaptive Mixup and Neural Collapse

Trung-Anh Dang¹, Vincent Nguyen¹, Ngoc-Son Vu², Christel Vrain¹

¹Université d'Orléans, INSA CVL, LIFO UR 4022, Orléans, France

²ETIS - CY Cergy Paris University, ENSEA, CNRS, France

trung-anh.dang@univ-orleans.fr, vincent.nguyen@univ-orleans.fr, son.vu@ensea.fr, christel.vrain@univ-orleans.fr

Abstract

While most continual learning methods focus on mitigating forgetting and improving accuracy, they often overlook the critical aspect of network calibration, despite its importance. Neural collapse, a phenomenon where last-layer features collapse to their class means, has demonstrated advantages in continual learning by reducing feature-classifier misalignment. Few works aim to improve the calibration of continual models for more reliable predictions. Our work goes a step further by proposing a novel method that not only enhances calibration but also improves performance by reducing overconfidence, mitigating forgetting, and increasing accuracy. We introduce Sphere-Adaptive Mixup (SAMix), an adaptive mixup strategy tailored for neural collapse-based methods. SAMix adapts the mixing process to the geometric properties of feature spaces under neural collapse, ensuring more robust regularization and alignment. Experiments show that SAMix significantly boosts performance, surpassing SOTA methods in continual learning while also improving model calibration. SAMix enhances both across-task accuracy and the broader reliability of predictions, making it a promising advancement for robust continual learning systems.

1 Introduction

To achieve human-like lifelong learning, deep neural networks (DNNs) must support continual learning (CL), the ability to acquire new knowledge incrementally while retaining previously learned information. However, a major challenge is catastrophic forgetting (McCloskey and Cohen 1989; Robins 1995), where new learning disrupts old knowledge. In response, CL has rapidly evolved with numerous approaches (Rusu et al. 2016; Cha, Lee, and Shin 2021; Pourcel, Vu, and French 2022; Wen et al. 2024; Tang et al. 2024; Dang et al. 2025), primarily aimed at balancing adaptation to new data (plasticity) and retention of past knowledge (stability). Compared to joint training (Yoon et al. 2018; Buzzega et al. 2020; Tiwari et al. 2022), decoupling representation and classifier learning has shown superior performance in both continual supervised (Cha, Lee, and Shin 2021; Wen et al. 2024; Li et al. 2024a; Dang et al. 2025) and self-supervised learning (Fini et al. 2022; Cha, Cho, and Moon 2024; Madaan et al. 2022; Mushtaq et al. 2024). Among these, **mixup** (Zhang et al. 2018) has emerged as a simple yet effective technique, primarily applied in continual self-supervised learning (Madaan

et al. 2022; Mushtaq et al. 2024) to promote smoother task transitions and increase sample diversity, especially for old samples in buffers. Beyond reducing forgetting, mixup also acts as a **calibration** method, aligning predicted confidence scores with actual accuracy. In DNNs, calibration reflects prediction reliability - a crucial factor for safety-sensitive applications that often require CL, such as medical diagnosis (Jiang et al. 2012) and autonomous driving (Grigorescu et al. 2020), where unreliable predictions can pose serious risks. However, the role of mixup in mitigating overconfidence and enhancing CL performance remains underexplored.

Neural collapse (NC), where last-layer features converge to their class means during training, has attracted significant attention in DNNs across both *static* and *dynamic* (continual) learning scenarios (Lu and Steinerberger 2020; Fang et al. 2021; Ji et al. 2022; Zhou et al. 2022; Fisher, Meng, and Popyan 2024). Most NC-based methods rely on the dot-regression loss (DR) (Yang et al. 2022), which enforces feature alignment with fixed class prototypes to enhance class separation and reduce misalignment between features and classifiers. Recently, focal neural collapse contrastive (FNC²) (Dang et al. 2025) loss was introduced to leverage NC more flexibly in CL. Unlike DR, which rigidly aligns features with class prototypes, FNC² optimizes feature relationships, enhancing intra-class diversity and improving generalization. While NC-based methods effectively improve accuracy and mitigate forgetting, their impact on calibration remains unexplored, as does the effect of calibration in NC-based methods on overall model performance. Indeed, as shown in (Li et al. 2024b; Hwang, Kim, and Whang 2025), beyond performance, CL models must also produce well-calibrated predictions. However, existing attempts at calibration in CL remain relatively simple and leave much room for improvement.

In this work, we address both across-task accuracy and the overlooked challenge of calibration in continual learners. We conduct a comparative analysis of NC-based methods, examining their ability to balance performance and reliability in CL. Our main contributions are summarized as:

1. We propose Sphere-Adaptive Mixup (SAMix), a simple yet effective method to improve calibration, mitigate forgetting, and boost accuracy in NC-based CL. SAMix leverages spherical linear interpolation of fixed ETF (Equiangular Tight Frame) prototypes to gener-

ate adaptive mixed prototypes, enhancing representation learning and smoothing decision boundaries.¹ We also introduce new metrics to evaluate calibration and overconfidence in CL, using them to assess the reliability of NC-based methods.

2. We provide theoretical analyses to compare different NC-based methods for handling mixed samples and validate our findings through empirical results.
3. Through extensive experiments, we show that our calibration strategy significantly enhances network calibration, reduces overconfidence, and improves performance in CL. Notably, our approach with a novel method achieves SOTA results across multiple datasets, both with and without memory, in most experimental settings.

2 Related Work

2.1 Continual Learning

CL algorithms can be categorized into two main paradigms: pretrained-based and training-from-scratch. Pretrained methods (Wang et al. 2022b,a; Smith et al. 2023; Liu and Yang 2025) leverage large datasets for general representations, while training-from-scratch approaches suit resource-limited settings. These latter algorithms can be grouped into: **Architecture**-based methods (Rusu et al. 2016; Yoon et al. 2018; Li et al. 2019), which allocate task-specific parameters or expand networks; **Regularization**-based methods (Zenke, Poole, and Ganguli 2017; Jung et al. 2020; Fini et al. 2022; Park et al. 2019; Tang et al. 2024; Dang et al. 2025), which constrain weight updates to preserve past knowledge; and **Rehearsal**-based or **replay**-based methods (Madaan et al. 2022; Buzzega et al. 2020; Cha, Lee, and Shin 2021; Wen et al. 2024; Mushtaq et al. 2024), which replay stored data or use generative models.

A primary challenge in CL is the plasticity-stability dilemma - balancing the integration of new knowledge (plasticity) with the retention of past information (stability). Regularization-based methods often address this via knowledge distillation (Hinton, Vinyals, and Dean 2015), which preserves prior knowledge during training. This may involve intermediate features (Hou et al. 2019) or final outputs (Fini et al. 2022; Cha, Cho, and Moon 2024). Recent advances extend distillation to relational knowledge, such as instance-wise relation distillation (IRD) in Co²L (Cha, Lee, and Shin 2021) and prototype-instance relation distillation (PRD) in CCLIS (Li et al. 2024a). Building on these, (Dang et al. 2025) proposes hardness-softness distillation (HSD), combining IRD and a variant of PRD for fixed prototypes, achieving superior performance. In this work, we adopt HSD to preserve past knowledge through relational consistency with fixed prototypes.

Remarks. While most CL methods aim to reduce forgetting and boost accuracy, they often overlook the crucial aspect of calibration. We address this gap by proposing a sim-

¹We note that (Li et al. 2024b; Hwang, Kim, and Whang 2025) aims to calibrate CL models for more reliable predictions, whereas our work goes further by proposing a method that enhances calibration and also mitigates forgetting, and improves accuracy.

ple yet effective calibration method and evaluating its impact on both calibration and performance across tasks.

2.2 Mixup

Mixup (Zhang et al. 2018) is a data augmentation strategy based on the principle of vicinal risk minimization (Chapelle et al. 2000), which interpolates linearly between example pairs and their corresponding labels. The equation of mixup is defined as:

$$\tilde{\mathbf{x}}_{ij} = \lambda \mathbf{x}_i + (1 - \lambda) \mathbf{x}_j \quad (1)$$

$$\tilde{\mathbf{y}}_{ij} = \lambda \mathbf{y}_i + (1 - \lambda) \mathbf{y}_j \quad (2)$$

where $(\mathbf{x}_i, \mathbf{y}_i)$, $(\mathbf{x}_j, \mathbf{y}_j)$ are two random pairs of samples and one-hot labels drawn from the training data, and $\lambda \in [0, 1] \sim \text{Beta}(\alpha, \alpha)$, $\alpha \in (0, \infty)$. With simplicity and ease of deployment, mixup has emerged as a well-known method, used widely in both supervised learning (Guo, Mao, and Zhang 2019; Verma et al. 2019) and unsupervised learning (Kim et al. 2020; Ren et al. 2022; Shen et al. 2022) to prevent overfitting and to improve generalization. Moreover, (Thulasidasan et al. 2019; Noh et al. 2023) show that mixup-trained DNNs are significantly better calibrated, with softmax scores closely reflecting actual correctness likelihood.

Mixup in CL. Mixup has recently been used in CL by combining current task samples with random memory instances to promote linearity across tasks. Most studies focus on self-supervised settings (Madaan et al. 2022; Mushtaq et al. 2024), where mixup serves both as an augmentation technique to increase the number of training samples, especially old ones in memory, and as a regularizer to distill knowledge and reduce forgetting.

Remarks. Like traditional mixup and its CL adaptations, we generates new samples via linear interpolation. However, instead of mixing labels, we interpolate class prototypes on a hypersphere. While mixup benefits in CL, its impact on calibration remains underexplored. This work bridges this gap by showing how our method improves calibration, reduces overconfidence, and still boosts accuracy.

2.3 Neural Collapse

Neural collapse (NC) (Papyan, Han, and Donoho 2020) is a phenomenon observed during the final stage of DNN training, where last-layer features and classifier form a structured geometric pattern on a balanced dataset, aligning with a simplex Equiangular Tight Frame (ETF). Building on this foundation, subsequent studies have proven NC is globally optimal in balanced training with cross-entropy (Lu and Steinerberger 2020; Zhu et al. 2021; Ji et al. 2022) and mean squared error (Poggio and Liao 2020; Han, Papyan, and Donoho 2022; Zhou et al. 2022) losses. In addition, (Yang et al. 2022) try to induce NC by fixing the classifier under imbalanced training, addressing the issue of misalignment between features and classifier.

NC and Mixup. A recent study (Fisher, Meng, and Papyan 2024) shows that mixup induces a distinct geometric structure. In cross-entropy classifiers with one-hot labels, same-class mixed samples align with a simplex ETF, while cross-class ones form smooth channels along decision

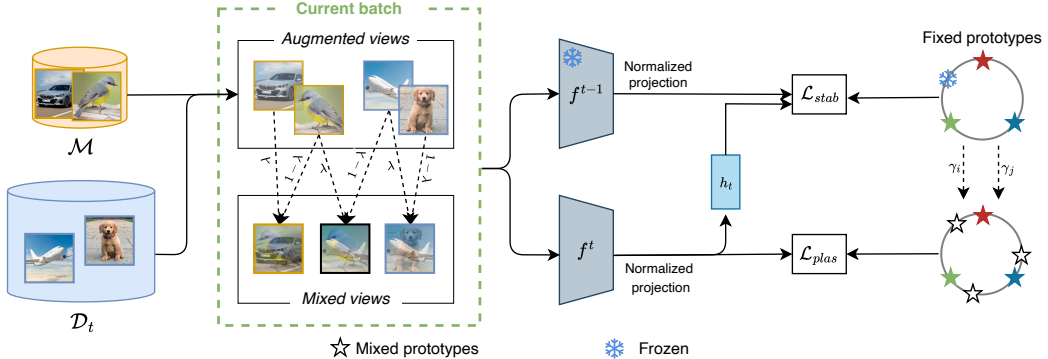


Figure 1: Illustration of our proposed method.

boundaries, leading to *smoother separation*. This effect persists even when classifier weights are fixed as a simplex ETF, enhancing both generalization and calibration.

Inducing NC for CL. Inspired by (Galanti, Gyorgy, and Hutter 2022), which showed that NC persists under transfer to new samples or classes, many CL studies (Yang et al. 2023a,b) leverage NC via DR loss (Yang et al. 2022) to reduce forgetting. These methods fix a simplex ETF as classifier prototypes across tasks and align them with sample features. Meanwhile, **contrastive** learning has gained traction in CL, with remarkable performance from models like Co²L (Cha, Lee, and Shin 2021), CILA (Wen et al. 2024), and CCLIS (Li et al. 2024a). (Dang et al. 2025) introduces FNC², a contrastive loss that explores NC in CL. Here, we employ both FNC² and DR losses in our analysis.

3 Methodology

3.1 Preliminaries

The general supervised CL problem is split in T tasks. Each task $t \in \{1, \dots, T\}$ has a dataset $\mathcal{D}_t = \{(\mathbf{x}_i, y_i)\}_{i=1}^{N_t}$ with N_t pairs and a distinct class set \mathcal{C}_t . The total number of classes across tasks: $\sum_{t=1}^T |\mathcal{C}_t| = K$. We focus on two popular CL settings: class-incremental learning (Class-IL) and task-incremental learning (Task-IL), where tasks have disjoint class labels: $\mathcal{C}_t \cap \mathcal{C}_{t'} = \emptyset$ for $t \neq t'$. In Task-IL, the task label is available during testing. Each batch \mathcal{B} of N samples is augmented to $2N$ views. After augmentation, each image \mathbf{x}_i is passed through the feature extractor f and projector g to obtain the output $\mathbf{z}_i = (g \circ f)_{\theta}(\mathbf{x}_i)$ on the unit d -dimensional sphere (with θ denoting model parameters).

3.2 Overall Architecture

Our method is illustrated in Figure 1. We adopt a two-stage learning framework that enhances invariant representations across tasks. As in prior work (Cha, Lee, and Shin 2021; Wen et al. 2024; Dang et al. 2025), we incorporate two main losses: (1) plasticity loss \mathcal{L}_{plas} to learn new knowledge and (2) stability loss \mathcal{L}_{stab} to distill past information. We predefine a set of **fixed, non-learnable** class prototypes $\mathbf{P} = \{\mathbf{p}_i\}_{i=1}^K$, structured as a simplex ETF. These prototypes are shared across tasks and are used in both loss

terms during training. To encourage smoother and more linear transitions between tasks, we introduce SAMix, an adaptive mixup strategy tailored for NC-based approaches. In replay settings, a memory buffer \mathcal{M} is maintained using reservoir sampling (Vitter 1985) to store past samples.

Specifically, during training, each batch consists of samples from the current dataset \mathcal{D}_t and the buffer \mathcal{M} . These are augmented and randomly selected and mixed along with their corresponding prototypes. All views (original and mixed) are then fed into the current model f^t for computing \mathcal{L}_{plas} , and into the frozen past model f^{t-1} for \mathcal{L}_{stab} . Mixed prototypes are used solely for \mathcal{L}_{plas} while predefined fixed prototypes are involved in both losses. An overview of the full algorithm is provided in the Appendix.

3.3 Sphere-Adaptive Mixup

Our new mixup method utilizes mixed samples and prototypes to improve smooth boundaries in representation learning and enhance calibration. Each batch is drawn from the current task data \mathcal{D}_t and the memory buffer \mathcal{M} . Given two random samples (\mathbf{x}_i, y_i) and (\mathbf{x}_j, y_j) with corresponding prototypes \mathbf{p}_{y_i} and \mathbf{p}_{y_j} , we generate a mixed sample $\tilde{\mathbf{x}}_{ij}$ as in Eq. (1). Unlike original mixup (Zhang et al. 2018), which combines target labels as in Eq. (2), we generate new prototypes based on the mixing coefficient λ . To generate mixed prototypes, several works (Yang et al. 2022; Fisher, Meng, and Popyan 2024) use linear interpolation, defined as:

$$\tilde{\mathbf{p}}_{ij} = \lambda \mathbf{p}_{y_i} + (1 - \lambda) \mathbf{p}_{y_j} \quad (3)$$

However, since both the features $\mathbf{z}_i, \mathbf{z}_j$ of the corresponding samples $\mathbf{x}_i, \mathbf{x}_j$ and the prototypes $\mathbf{p}_{y_i}, \mathbf{p}_{y_j}$ lie on the unit hypersphere, interpolating mixed prototypes using Eq. (3) is inappropriate. As illustrated in Figure 2a, using linear interpolation causes the mixed prototype lying on the linear path between two prototypes, rather than on the unit hypersphere. The mixed prototype $\tilde{\mathbf{p}}_{ij}$ resides on the unit hypersphere only if its l_2 -norm satisfies: $\|\tilde{\mathbf{p}}_{ij}\|_2 = 1$. Based on Eq. (3), we compute its squared l_2 -norm as:

$$\begin{aligned} \|\tilde{\mathbf{p}}_{ij}\|_2^2 &= \|\lambda \mathbf{p}_{y_i} + (1 - \lambda) \mathbf{p}_{y_j}\|_2^2 \\ &= \lambda^2 \|\mathbf{p}_{y_i}\|_2^2 + 2\lambda(1 - \lambda) \langle \mathbf{p}_{y_i} \cdot \mathbf{p}_{y_j} \rangle \\ &\quad + (1 - \lambda)^2 \|\mathbf{p}_{y_j}\|_2^2 \end{aligned} \quad (4)$$

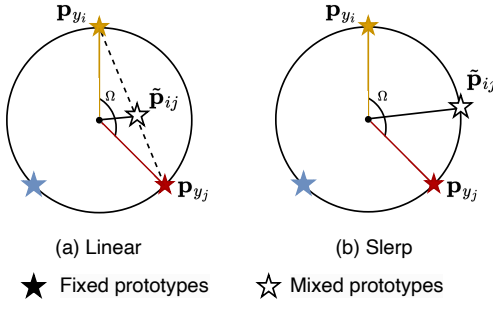


Figure 2: Linear interpolation and Slerp.

Since $\|\mathbf{p}_{y_i}\|_2^2 = 1$ and $\|\mathbf{p}_{y_j}\|_2^2 = 1$, Eq. (4) simplifies to:

$$\|\tilde{\mathbf{p}}_{ij}\|_2^2 = \lambda^2 + (1 - \lambda)^2 + 2\lambda(1 - \lambda)\cos\Omega \quad (5)$$

where $\langle \cdot \rangle$ is the cosine similarity, $\Omega = \angle(\mathbf{p}_{y_i}, \mathbf{p}_{y_j})$. From Eq. (5), $\tilde{\mathbf{p}}_{ij}$ only remain $l2$ -normalized when $\cos\Omega = 1$, meaning \mathbf{p}_i and \mathbf{p}_j are in the same direction. Since each mixed prototype is created from two prototypes corresponding to two randomly selected sample pairs, these two prototypes point in the same direction only if the two selected samples are from the same class. In this case, they are identical and the mixed prototype is the prototype of this class. Otherwise with two samples from different classes, the angle $\Omega \neq 0$, leading to $\|\tilde{\mathbf{p}}_{ij}\| \neq 1$, the mixed prototype is not on the unit hypersphere.

To ensure that mixed prototypes always remain on the unit hypersphere, we use Spherical Linear Interpolation (Slerp) (Shoemake 1985) instead of linear interpolation. A geometric visualization of this approach is shown in Figure 2b. The hypersphere-interpolated prototype $\tilde{\mathbf{p}}_{ij}$ is:

$$\tilde{\mathbf{p}}_{ij} = \gamma_i \mathbf{p}_{y_i} + \gamma_j \mathbf{p}_{y_j} \quad (6)$$

where $\gamma_i = \frac{\sin(\lambda\Omega)}{\sin\Omega}$ and $\gamma_j = \frac{\sin((1-\lambda)\Omega)}{\sin\Omega}$.

Note that, due to the random selection of sample pairs, both mixed samples and mixed prototypes *vary across batches*. We refer to this adaptive mixup of fixed prototypes on a hypersphere as Sphere-Adaptive Mixup (SAMix). Like the original prototypes, the mixed prototypes are **fixed and not updated** during training.

3.4 Integration of SAMix into NC-based Methods

We note that mixed samples from SAMix are used only in \mathcal{L}_{plas} and *not* in \mathcal{L}_{stab} . On the first hand, mixed samples are designed to enhance plasticity for new tasks (smoother transitions between tasks). On the other hand, \mathcal{L}_{stab} focuses on preserving old knowledge: when using relation-based distillation techniques, such as instance-wise or instance-prototype relationships, only the fixed prototypes and original samples should be used, not the mixed ones. This approach aligns with the work in (Beyer et al. 2022), which suggests that a “patient” teacher is ideal for knowledge distillation, meaning mixed samples, and thus mixed class prototypes are unnecessary for distillation.

SAMix is designed to complement any NC-based method that relies on fixed prototypes. In this work, we investigate

SAMix with two prominent NC-based plastic losses: dot-regression (DR) (Yang et al. 2022) and the recent focal neural collapse contrastive (FNC²) (Dang et al. 2025) which are respectively defined in Eq. (7) and Eq. (8):

$$\mathcal{L}_{DR} = \frac{1}{2N} \sum_{i=1}^{2N} \frac{1}{2} (\langle \mathbf{z}_i \cdot \mathbf{p}_{y_i} \rangle - 1)^2 \quad (7)$$

$$\begin{aligned} \mathcal{L}_{FNC^2} = - \sum_{i=1}^{2N} \frac{1}{|P(i)| + 1} & \left(\sum_{\mathbf{z}_j \in P(i)} (1 - c_{ij})^\gamma \log(c_{ij}) \right. \\ & \left. + (1 - r_i)^\gamma \log(r_i) \right) \end{aligned} \quad (8)$$

with $c_{ij} = \frac{e^{\langle \mathbf{z}_i \cdot \mathbf{z}_j \rangle / \tau}}{A + \sum_{k \neq i} e^{\langle \mathbf{z}_i \cdot \mathbf{z}_k \rangle / \tau}}$, $r_i = \frac{e^{\langle \mathbf{z}_i \cdot \mathbf{p}_{y_i} \rangle / \tau}}{A + \sum_{\mathbf{p}_l \in \mathbf{P}_{1:t-1}} e^{\langle \mathbf{z}_i \cdot \mathbf{p}_l \rangle / \tau}}$, and $A = \sum_{k \neq i} e^{\langle \mathbf{z}_i \cdot \mathbf{z}_k \rangle / \tau} + \sum_{\mathbf{p}_l \in \mathbf{P}_{1:t-1}} e^{\langle \mathbf{z}_i \cdot \mathbf{p}_l \rangle / \tau}$. Here, $P(i)$ is the set of indices for positive views (i.e., same-class views) of the anchor \mathbf{x}_i in the current batch, and τ is the temperature factor; \mathbf{p}_{y_i} is the prototype of class y_i , and $\mathbf{P}_{1:t-1}$ denotes the set of prototypes from past tasks.

Training batch composition. Each batch includes $2N$ normal samples (see Sec. 3.1) and $2N$ mixed samples ($4N$ total). Despite the increased batch size, our method achieves significant performance gains with little extra time and remains effective even with smaller batches (see Appendix).

Mixed samples in plasticity loss.

- For DR-based methods, we apply the DR loss to both normal samples (\mathbf{z}) and mixed samples ($\tilde{\mathbf{z}}$), yielding $\mathcal{L}_{plas} = \mathcal{L}_{DR}(\mathbf{z}) + v\mathcal{L}_{DR}(\tilde{\mathbf{z}})$, where v is a trade-off factor.
- For FNC²-based methods, we apply \mathcal{L}_{FNC^2} only to normal samples and use \mathcal{L}_{DR} to mixed samples, resulting in $\mathcal{L}_{plas} = \mathcal{L}_{FNC^2}(\mathbf{z}) + \iota\mathcal{L}_{DR}(\tilde{\mathbf{z}})$, with ι as a balancing hyperparameter. This means that we do not use mixed samples as negative in contrastive loss.

Explanation. Unlike prior contrastive learning work (Zhang et al. 2021) that uses mixup to create hard negative samples, SAMix follows the original mixup approach (Zhang et al. 2018), drawing coefficients $\lambda \in [0, 1]$ from a Beta(α, α) distribution and pairing samples randomly, regardless of class. This can produce near-positive mixed samples (e.g., when λ is close to 0 or 1, or when pairs are from the same class), which may disrupt contrastive alignment (Wang and Isola 2020) if treated as negatives. To prevent this, we avoid using mixed samples as negative views in losses like FNC². Moreover, applying a contrastive loss like FNC² to mixed samples is suboptimal, since each mixed sample forms a single-instance minority class, and as in the Appendix proof, this approach can even disrupt the mixed-up configuration (Fisher, Meng, and Popyan 2024).

- Mixed samples in DR loss. For the DR loss (see Eq. (7)), mixed samples are directly incorporated without modification. For each of the $2N$ mixed samples in the batch, we replace the feature \mathbf{z}_i and prototype \mathbf{p}_{y_i} with the mixed sample feature $\tilde{\mathbf{z}}_{ij}$ and mixed prototype $\tilde{\mathbf{p}}_{ij}$, respectively, ensuring seamless integration into the loss computation.

Stability loss. For \mathcal{L}_{stab} , we use hardness-softness distillation (HSD) (Dang et al. 2025), which surpasses instance-wise relation distillation (Cha, Lee, and Shin 2021) and

sample-prototype relation distillation (S-PRD) (Dang et al. 2025) in preserving old knowledge (see Appendix for loss definitions). We refer to the approach in (Dang et al. 2025) as Focal Contrastive Neural Collapse Continual Learning (FC-NCCL). Besides, we propose a novel method using DR for plasticity and HSD for stability, which we refer to Tightly Aligned Neural Collapse Continual Learning (TA-NCCL).

3.5 Expected Outcome Hypothesis

We hypothesize the following results, to be validated in Sec. 4, confirming SAMix’s role in improving CL performance and calibration, and in reducing overconfidence.

(a) H1: Performance without SAMix. FC-NCCL is expected to outperform TA-NCCL, as it better preserves within-class distributions during representation learning (Dang et al. 2025). It is also anticipated to outperform TA-NCCL in calibration, since its FNC² loss already integrates temperature scaling and focal loss, two well-established calibration techniques (Guo et al. 2017; Lin et al. 2017).

(b) H2: Limited benefit of SAMix for FNC². We hypothesize that SAMix provides limited benefits for FNC² in FC-NCCL when FNC² is applied to normal samples and DR to mixed ones. As a contrastive loss, FNC² benefits from more negative samples (Chen et al. 2020), which SAMix does not provide. Therefore, we predict that any performance gains from integrating SAMix primarily come from the DR loss, as it better leverages mixed samples. In contrast, FNC² relies on a large number of negative samples, which SAMix does not address.

(c) H3: Significant benefit of SAMix for DR. In contrast, we expect DR, which operates on mixed samples, to fully benefit from SAMix. Unlike FNC², which considers both sample-sample and sample-prototype contrastive relationships for flexible clustering, DR only focuses on sample-prototype relations, resulting in distinct but less flexible clusters. However, when SAMix is applied, the decision boundaries become smoother. As mentioned in (Fisher, Meng, and Papyan 2024), using mixup can create new configurations with mixed samples, significantly enhancing representation learning. We expect this will allow DR to learn more robust representations, improve generalization, and perform better on both the current task and across tasks in CL, while also mitigating forgetting.

(d) H4: Enhanced calibration and reduced overconfidence. We further hypothesize that SAMix improve calibration and reduce overconfidence for both FC-NCCL and TA-NCCL, at least on the current task. This stems from the inherent calibration properties of mixup, which SAMix inherits. SAMix’s ability to smooth decision boundaries and create mixed samples will lead to more calibrated predictions, helping to reduce overconfidence.

4 Experiments

4.1 Datasets and Implementation details

Datasets. We use three standard CL datasets widely used in literature for fair comparison under Class-IL and Task-IL settings (3.1): Seq-Cifar-10 and Seq-Cifar-100 (Krizhevsky and Hinton 2009), and Seq-Tiny-ImageNet (Le and Yang

2015). Seq-Cifar-10 has 5 tasks with 2 classes each; Seq-Cifar-100 and Seq-Tiny-ImageNet each have 5 and 10 tasks with 20 classes per task, respectively.

Implementation details. We utilize ResNet-18 (He et al. 2016) as the backbone, omitting the final layer as in (Cha, Lee, and Shin 2021; Fini et al. 2022; Dang et al. 2025; Li et al. 2024a). Following (Chen et al. 2020; Zbontar et al. 2021; Cha, Lee, and Shin 2021), we add a two-layer projection MLP g^t to map backbone features into a d -dimensional space ($d = 128$ for Seq-Cifar-10/100, $d = 256$ for Seq-Tiny-ImageNet). For distillation, as in (Fini et al. 2022), we use a predictor h^t with the same architecture as g^t to align current and past feature spaces. Besides, we use buffer sizes of 0, 200, and 500. For evaluation, following (Cha, Lee, and Shin 2021; Wen et al. 2024; Dang et al. 2025), we train a classifier s^t on top of the frozen encoder f^t for 100 epochs, using samples from the last-task training dataset \mathcal{D}_t and buffer \mathcal{M} . As in (Cha, Lee, and Shin 2021), no buffer is used during representation learning in the memory-free setting, but 200 auxiliary samples are still needed to only train the classifier for all datasets. Experiments are conducted on a NVIDIA Quadro GV100 GPU with 256GB RAM, Ubuntu 20.04, and PyTorch 1.12.1 (Paszke et al. 2019).

Considered methods. We evaluate SAMix across the SOTA NC-based methods: FC-NCCL (Dang et al. 2025) and TA-NCCL. We also consider recent baselines, including CCLIS (Li et al. 2024a), CILA (Wen et al. 2024), and other well-known supervised methods such as ER (Riemer et al. 2019), DER (Buzzega et al. 2020), Co²L (Cha, Lee, and Shin 2021), and GCR (Tiwari et al. 2022).

Evaluation metrics. As in prior work (Cha, Lee, and Shin 2021; Fini et al. 2022; Wen et al. 2024; Dang et al. 2025; Li et al. 2024a), we report Average Accuracy (AA) (Chaudhry et al. 2018) across all tasks on the test dataset after learning the final task T : $AA = \frac{1}{T} \sum_{k=1}^T A_{T,k}$. In addition, we use Average Forgetting (Chaudhry et al. 2018) to measure how much the model forgets previous tasks (see Appendix).

Calibration metrics. To assess network calibration, we use the metrics from (Guo et al. 2017). Predictions are divided into M interval equal-sized bins, with B_m representing the set of samples whose prediction scores (the winning softmax score) fall into bin m . The accuracy and confidence of B_m are defined as: $acc(B_m) = \frac{1}{|B_m|} \sum_{i \in B_m} \mathbf{1}(\hat{y}_i = y_i)$; $conf(B_m) = \frac{1}{|B_m|} \sum_{i \in B_m} \hat{p}_i$, where \hat{p}_i is the confidence (winning score) of sample i . The Expected Calibration Error (ECE) is defined as: $ECE = \sum_{m=1}^M \frac{|B_m|}{n} |acc(B_m) - conf(B_m)|$. We also use the Overconfidence Error (OE) metric (Thulasidasan et al. 2019), essential for high-risk applications where confidently incorrect predictions are critical: $OE = \sum_{m=1}^M \frac{|B_m|}{n} [conf(B_m) \times \max(conf(B_m) - acc(B_m), 0)]$. This metric heavily penalizes overconfident predictions when confidence exceeds accuracy.

Building on these metrics, we propose new metrics which are adaptive to CL: **Average Expected Calibration Error** (AECE) and **Average Overconfidence Error** (AOE):

$$AECE = \frac{1}{T} \sum_{k=1}^T ECE_{T,k}; AOE = \frac{1}{T} \sum_{k=1}^T OE_{T,k} \quad (9)$$

Buffer	Dataset Scenario	Venue	Seq-Cifar-100		Seq-Tiny-ImageNet		Seq-Cifar-10	
			Class-IL	Task-IL	Class-IL	Task-IL	Class-IL	Task-IL
0	Co ² L	ICCV'21	26.89±0.78	51.91±0.63	13.43±0.57	40.21±0.68	58.89±2.61	86.65±1.05
	FC-NCCL	WACV'25	32.57±0.55	57.87±0.62	14.54±0.52	43.81±0.47	69.26±0.32	94.41±0.43
	FC-NCCL + SAMix		40.15±0.48	64.96±0.72	15.72±0.34	44.65±0.59	66.47±1.26	93.09±1.13
	Ours		33.48±0.22	60.79±0.54	10.88±0.51	35.61±0.41	64.83±0.56	94.54±0.48
	Ours + SAMix		44.41±0.35	70.33±0.48	17.19±0.48	45.12±0.73	70.32±0.43	95.89±0.74
200	ER	ICLR'19	21.78±0.48	60.19±1.01	8.49±0.16	38.17±2.00	44.79±1.86	91.19±0.94
	DER	NeurIPS'20	31.23±1.38	63.09±1.09	11.87±0.78	40.22±0.67	61.93±1.79	91.40±0.92
	Co ² L	ICCV'21	27.38±0.85	53.94±0.76	13.88±0.40	42.37±0.74	65.57±1.37	93.43±0.78
	GCR	CVPR'22	33.69±1.40	64.24±0.83	13.05±0.91	42.11±1.01	64.84±1.63	90.80±1.05
	CILA	ICML'24	-	-	14.55±0.39	44.15±0.70	67.06±1.59	94.29±0.24
500	CCLIS	AAAI'24	42.39±0.37	72.93±0.46	16.13±0.19	48.29±0.78	74.95±0.61	96.20±0.26
	FC-NCCL	WACV'25	34.04±0.42	59.46±0.65	15.52±0.53	44.59±0.72	72.63±0.78	95.31±0.32
	FC-NCCL + SAMix		41.92±0.68	66.36±0.70	17.58±0.35	46.83±0.59	69.31±0.68	94.93±0.74
	Ours		36.67±1.18	64.64±1.37	11.04±0.29	35.49±0.62	66.78±0.23	93.98±0.17
	Ours + SAMix		46.95±0.71	73.48±0.29	18.39±0.38	49.51±0.83	73.25±0.54	96.68±0.32
	(+10.93 ▲)	(+9.54 ▲)	(+6.31 ▲)	(+9.51 ▲)	(+5.49 ▲)	(+1.35 ▲)		
	ER	ICLR'19	27.66±0.61	66.23±1.52	9.99±0.29	48.64±0.46	57.74±0.27	93.61±0.27
	DER	NeurIPS'20	41.36±1.76	71.73±0.74	17.75±1.14	51.78±0.88	70.51±1.67	93.40±0.39
	Co ² L	ICCV'21	37.02±0.76	62.44±0.36	20.12±0.42	53.04±0.69	74.26±0.77	95.90±0.26
	GCR	CVPR'22	45.91±1.30	71.64±2.10	19.66±0.68	52.99±0.89	74.69±0.85	94.44±0.32
	CILA	ICML'24	-	-	20.64±0.59	54.13±0.72	76.03±0.79	96.40±0.21
	CCLIS	AAAI'24	46.08±0.67	74.51±0.38	22.88±0.40	57.04±0.43	78.57±0.25	96.18±0.43
	FC-NCCL	WACV'25	40.25±0.58	65.85±0.44	20.31±0.34	53.46±0.59	75.51±0.52	96.14±0.25
	FC-NCCL + SAMix		47.87±0.57	72.95±1.05	20.71±0.43	54.25±0.57	75.87±0.66	95.35±0.39
	Ours		41.72±0.16	68.42±0.33	16.05±0.36	44.22±0.89	68.71±0.59	94.68±0.52
	Ours + SAMix		55.85±0.61	79.02±0.78	22.95±0.47	57.13±0.32	78.62±0.38	96.98±0.57
	(+14.13 ▲)	(+10.60 ▲)	(+6.90 ▲)	(+12.91 ▲)	(+9.91 ▲)	(+2.30 ▲)		

Table 1: Comparison of our method with supervised baselines at memory sizes 200 and 500, averaged over 5 trials from 5 different seeds (best results in bold). ▲ indicates performance improvement when applying SAMix. (Ours: TA-NCCL method).

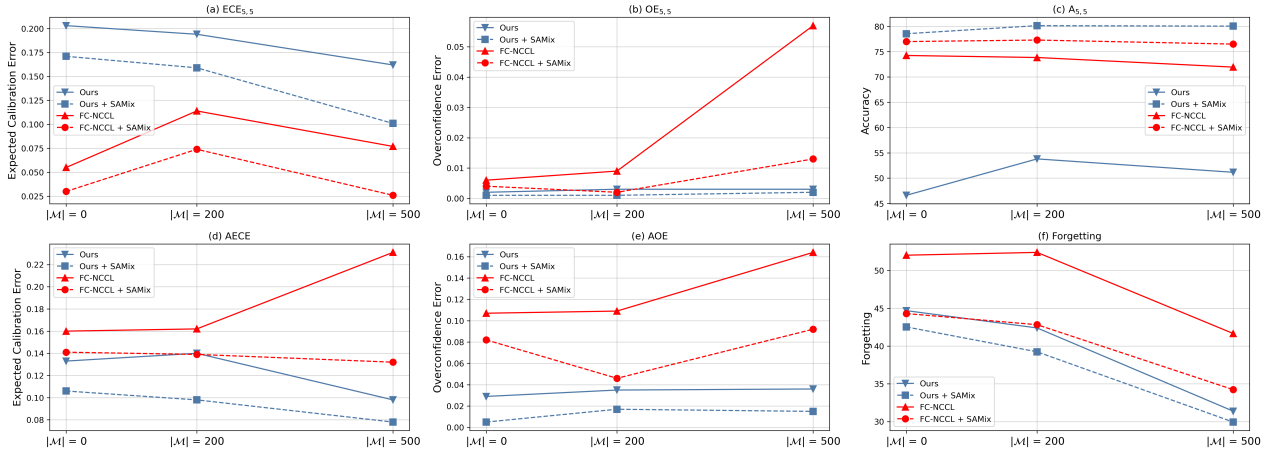


Figure 3: Results on Seq-Cifar100 with the Class-IL setting.

where $ECE_{T,k}$, $OE_{T,k}$ is the ECE, OE value of task k after learning the final task T correspondingly.

4.2 Main Results

Experimental results are shown in Table 1, where we report accuracies from baselines with published or available code.

Figure 3 presents $ECE_{5,5}$, $OE_{5,5}$, and $A_{5,5}$ on the final task ($T = 5$) (top row), and $AECE$, AOE , Forgetting across tasks (bottom row) on Seq-Cifar-100. These results highlight the impact of SAMix on FNC² and DR, as well as on calibration and performance. We evaluate these findings against the proposed hypotheses, focusing on FC-NCCL and TA-NCCL.

a) H1 - without SAMix. The hypothesis is **partially** validated. On Seq-Tiny-ImageNet and Seq-Cifar-10, FC-NCCL outperforms TA-NCCL in accuracy and calibration across buffer sizes, except in a few Task-IL cases where the results are nearly equivalent. This supports the hypothesis that preserving within-class distributions improves CL performance. The integration of temperature scaling and focal loss in FNC² yields better-calibrated predictions, as evidenced by FC-NCCL’s significantly lower $ECE_{5,5}$ compared to DR.

However, on Seq-Cifar-100, the trend reverses, with DR outperforming FNC² entirely, which contradicts the initial performance hypothesis. We attribute this to Cifar-100’s higher inter-class similarity (Bertinetto et al. 2019), stemming from its 100 classes grouped into 20 semantically related superclasses (e.g., vehicles, animals). In contrast, Tiny ImageNet contains 200 more diverse and ungrouped classes. This similarity in Cifar-100 may lead to greater class confusion, limiting the advantages of FC-NCCL. Moreover, as shown in Figure 3a, FNC² achieves lower $ECE_{5,5}$ on the current task, indicating better calibration than DR. However, with buffer usage, FC-NCCL shows higher $OE_{5,5}$ than TA-NCCL (see Figure 3b).

b) H2: Limited benefit of SAMix for FNC2. This hypothesis holds partially, as SAMix yields slight improvements on Seq-Tiny-ImageNet and even degrades performance on Seq-Cifar-10 with buffer sizes of 0 and 200. In methods using plasticity loss FNC², applying DR to mixed samples often shift the model’s focus toward blended artifacts rather than meaningful features, leading to forgetting. In contrast, on Seq-Cifar-100, SAMix significantly enhances FC-NCCL performance, which is attributed to the dataset’s high inter-class similarity (Bertinetto et al. 2019). In this case, SAMix refines class boundaries and boosts performance. Without it, performance drops substantially compared to DR-based, which further highlights its benefits.

c) H3: Significant benefit of SAMix for DR. Experimental results strongly support this hypothesis. With SAMix, TA-NCCL (relying on DR) outperforms FC-NCCL, whereas without SAMix, FC-NCCL performs comparably or slightly better. These results align with our analysis in Sec. 3.5, where DR benefits more from SAMix than FNC² because DR loss strictly pulls samples toward prototypes as optimal points, leading to better representation learning, smoother decision boundaries, and improved accuracy.

Notably, TA-NCCL with SAMix achieves SOTA results in most settings, except on Seq-Cifar-10 (Class-IL, buffer size 200), particularly on large, complex datasets with many classes as Seq-Cifar-100 and Seq-Tiny-ImageNet.

d) H4: Enhanced calibration and reduced overconfidence. Figure 3 shows that SAMix significantly reduces calibration error and overconfidence while improving performance on both the current task and across tasks, effectively mitigating forgetting for both FC-NCCL and TA-NCCL in

Buffer	Metrics	Method			
		FC-NCCL + SAMix		Ours + SAMix	
		Linear	Slerp	Linear	Slerp
0	AECE(\downarrow)	0.164	0.141 \blacktriangle	0.130	0.106 \blacktriangle
	AOE(\downarrow)	0.108	0.082 \blacktriangle	0.027	0.005 \blacktriangle
	AA(\uparrow)	38.39	40.15 \blacktriangle	42.36	44.41 \blacktriangle
200	AECE(\downarrow)	0.140	0.139 \blacktriangle	0.114	0.098 \blacktriangle
	AOE(\downarrow)	0.071	0.046 \blacktriangle	0.043	0.017 \blacktriangle
	AA(\uparrow)	39.03	41.92 \blacktriangle	43.76	46.95 \blacktriangle
500	AECE(\downarrow)	0.158	0.132 \blacktriangle	0.079	0.078 \blacktriangle
	AOE(\downarrow)	0.105	0.092 \blacktriangle	0.042	0.015 \blacktriangle
	AA(\uparrow)	45.94	47.87 \blacktriangle	53.96	55.85 \blacktriangle

Table 2: Comparison between Slerp and linear interpolation on Seq-Cifar-100. \blacktriangle indicates that Slerp performs better.

most cases.

Mixup only within the current task. Without memory, SAMix applies only to current-task classes but still effectively reduces calibration error and overconfidence error while boosting performance. This highlights SAMix’s potential for CL tasks with limited storage or strict data privacy constraints.

4.3 Ablation Studies

Effectiveness of using slerp in SAMix. We report ablation results in Table 2, comparing Slerp and linear interpolation when applying SAMix to both FC-NCCL and TA-NCCL on Seq-Cifar-100 with buffer sizes of 0, 200, and 500. Slerp yields better calibration and lower AOE in all cases than linear interpolation. Moreover, it also consistently improves accuracy at larger distances. These results support the use of Slerp in SAMix and align with our analysis in Sec. 3.3.

5 Conclusion

In this work, we explore the role of mixup in enhancing model calibration, reducing forgetting, and improving performance in Neural Collapse-based continual learning. We propose SAMix, an adaptive mixup strategy tailored for NC-based CL methods, and show its substantial benefits when paired with DR loss. SAMix significantly boosts CL model performance, achieving SOTA results on benchmark datasets such as Seq-Cifar-100 and Seq-Tiny-ImageNet. Moreover, it reduces calibration error and overconfidence across tasks, even in memory-free settings, making it particularly valuable under strict data privacy constraints.

However, a limitation exists: while SAMix improves performance and calibration, it is tailored to fixed prototype-based CL. Our experiments with dynamic prototype methods and traditional one-stage CL approaches reveal integration challenges: direct incorporation is either technically infeasible (e.g., in one-stage supervised CL) or degrades performance, as mixup on randomly initialized dynamic prototypes lacks meaningful impact, especially early in training. Although NC-based methods currently lead the field, this constraint highlights the need to extend SAMix to dynamic prototype-based methods like CCLIS (Li et al. 2024a).

References

Bertinetto, L.; Henriques, J. F.; Torr, P.; and Vedaldi, A. 2019. Meta-learning with differentiable closed-form solvers. In *International Conference on Learning Representations*.

Beyer, L.; Zhai, X.; Royer, A.; Markeeva, L.; Anil, R.; and Kolesnikov, A. 2022. Knowledge distillation: A good teacher is patient and consistent. In *CVPR*.

Buzzega, P.; Boschini, M.; Porrello, A.; Abati, D.; and Calderara, S. 2020. Dark Experience for General Continual Learning: a Strong, Simple Baseline. In *NeurIPS*.

Cha, H.; Lee, J.; and Shin, J. 2021. Co\$^2\$L: Contrastive Continual Learning. In *ICCV*.

Cha, S.; Cho, K.; and Moon, T. 2024. Regularizing with Pseudo-Negatives for Continual Self-Supervised Learning. In *ICML*.

Chapelle, O.; Weston, J.; Bottou, L.; and Vapnik, V. 2000. Vicinal Risk Minimization. In *NeurIPS*, volume 13. MIT Press.

Chaudhry, A.; Dokania, P. K.; Ajanthan, T.; and Torr, P. H. S. 2018. Riemannian Walk for Incremental Learning: Understanding Forgetting and Intransigence. In *ECCV*.

Chen, H.; Goldblum, M.; Wu, Z.; and Jiang, Y.-G. 2025. Adaptive Retention & Correction: Test-Time Training for Continual Learning. In *ICLR*.

Chen, T.; Kornblith, S.; Norouzi, M.; and Hinton, G. 2020. A simple framework for contrastive learning of visual representations. In *ICML*.

Dang, T.-A.; Nguyen, V.; Vu, N.-S.; and Vrain, C. 2025. Memory-efficient Continual Learning with Neural Collapse Contrastive. In *WACV*.

Fang, C.; He, H.; Long, Q.; and Su, W. J. 2021. Exploring deep neural networks via layer-peeled model: Minority collapse in imbalanced training. *PNAS*.

Fini, E.; da Costa, V. G. T.; Alameda-Pineda, X.; Ricci, E.; Alahari, K.; and Mairal, J. 2022. Self-Supervised Models are Continual Learners. In *CVPR*.

Fisher, Q.; Meng, H.; and Papyan, V. 2024. Pushing Boundaries: Mixup’s Influence on Neural Collapse. In *ICLR*.

Galanti, T.; Gyorgy, A.; and Hutter, M. 2022. On the Role of Neural Collapse in Transfer Learning. In *ICLR*.

Grigorescu, S.; Trasnea, B.; Cocias, T.; and Macesanu, G. 2020. A survey of deep learning techniques for autonomous driving. *Journal of Field Robotics*.

Guo, C.; Pleiss, G.; Sun, Y.; and Weinberger, K. Q. 2017. On Calibration of Modern Neural Networks. In *ICML*.

Guo, H.; Mao, Y.; and Zhang, R. 2019. MixUp as Locally Linear Out-Of-Manifold Regularization. In *AAAI*.

Han, X. Y.; Papyan, V.; and Donoho, D. L. 2022. Neural Collapse Under MSE Loss: Proximity to and Dynamics on the Central Path. In *ICLR*.

He, K.; Zhang, X.; Ren, S.; and Sun, J. 2016. Deep Residual Learning for Image Recognition. In *CVPR*.

Hinton, G. E.; Vinyals, O.; and Dean, J. 2015. Distilling the knowledge in a neural network. In *NIPS Workshops*.

Hou, S.; Pan, X.; Loy, C. C.; Wang, Z.; and Lin, D. 2019. Learning a Unified Classifier Incrementally via Rebalancing. In *CVPR*.

Hwang, S.-H.; Kim, M.; and Whang, S. E. 2025. T-CIL: Temperature Scaling using Adversarial Perturbation for Calibration in Class-Incremental Learning. In *CVPR*.

Ji, W.; Lu, Y.; Zhang, Y.; Deng, Z.; and Su, W. J. 2022. An Unconstrained Layer-Peeled Perspective on Neural Collapse. In *ICLR*.

Jiang, X.; Osl, M.; Kim, J.; and Ohno-Machado, L. 2012. Calibrating predictive model estimates to support personalized medicine. *Journal of the American Medical Informatics Association*.

Jung, S.; Ahn, H.; Cha, S.; and Moon, T. 2020. Continual Learning with Node-Importance based Adaptive Group Sparse Regularization. In *NeurIPS*.

Khosla, P.; Teterwak, P.; Wang, C.; Sarna, A.; Tian, Y.; Isola, P.; Maschinot, A.; Liu, C.; and Krishnan, D. 2020. Supervised contrastive learning. In *NeurIPS*.

Kim, S.; Lee, G.; Bae, S.; and Yun, S.-Y. 2020. MixCo: Mix-up Contrastive Learning for Visual Representation. In *NeurIPS*.

Krizhevsky, A.; and Hinton, G. 2009. Learning multiple layers of features from tiny images. Technical report, University of Toronto, Toronto.

Le, Y.; and Yang, X. S. 2015. Tiny ImageNet Visual Recognition Challenge.

Li, J.; Azizov, D.; Li, Y.; and Liang, S. 2024a. Contrastive Continual Learning with Importance Sampling and Prototype-Instance Relation Distillation. In *AAAI*.

Li, L.; Piccoli, E.; Cossu, A.; Bacci, D.; and Lomonaco, V. 2024b. Calibration of Continual Learning Models. In *CVPRW*.

Li, X.; Zhou, Y.; Wu, T.; Socher, R.; and Xiong, C. 2019. Learn to Grow: A Continual Structure Learning Framework for Overcoming Catastrophic Forgetting. In *ICML*.

Lin, T.-Y.; Goyal, P.; Girshick, R.; He, K.; and Dollár, P. 2017. Focal Loss for Dense Object Detection. In *ICCV*.

Liu, Y.; and Yang, M. 2025. SEC-Prompt:SEmantic Complementary Prompting for Few-Shot Class-Incremental Learning. In *CVPR*, 25643–25656.

Loshchilov, I.; and Hutter, F. 2017. SGDR: Stochastic Gradient Descent with Warm Restarts. In *ICLR*.

Lu, J.; and Steinerberger, S. 2020. Neural Collapse with Cross-Entropy Loss. *arXiv:2012.08465*.

Madaan, D.; Yoon, J.; Li, Y.; Liu, Y.; and Hwang, S. J. 2022. Representational Continuity for Unsupervised Continual Learning. In *ICLR*.

McCloskey, M.; and Cohen, N. J. 1989. Catastrophic Interference in Connectionist Networks: The Sequential Learning Problem. *Psychology of Learning and Motivation*.

Mushtaq, E.; Yaldiz, D. N.; Bakman, Y. F.; Ding, J.; Tao, C.; Dimitriadis, D.; and Avestimehr, S. 2024. CroMo-Mixup: Augmenting Cross-Model Representations for Continual Self-Supervised Learning. In *ECCV*.

Noh, J.; Park, H.; Lee, J.; and Ham, B. 2023. RankMixup: Ranking-Based Mixup Training for Network Calibration. In *ICCV*.

Papyan, V.; Han, X. Y.; and Donoho, D. L. 2020. Prevalence of neural collapse during the terminal phase of deep learning training. *PNAS*.

Park, D.; Hong, S.; Han, B.; and Lee, K. M. 2019. Continual Learning by Asymmetric Loss Approximation With Single-Side Overestimation. In *ICCV*.

Paszke, A.; Gross, S.; Massa, F.; Lerer, A.; Bradbury, J.; Chanan, G.; Killeen, T.; Lin, Z.; Gimelshein, N.; Antiga, L.; Desmaison, A.; Kopf, A.; Yang, E.; DeVito, Z.; Raison, M.; Tejani, A.; Chilamkurthy, S.; Steiner, B.; Fang, L.; Bai, J.; and Chintala, S. 2019. PyTorch: An Imperative Style, High-Performance Deep Learning Library. In *NeurIPS*.

Poggio, T.; and Liao, Q. 2020. Explicit regularization and implicit bias in deep network classifiers trained with the square loss. arXiv:2101.00072.

Pourcel, J.; Vu, N.-S.; and French, R. M. 2022. Online Task-free Continual Learning with Dynamic Sparse Distributed Memory. In *ECCV*.

Ren, S.; Wang, H.; Gao, Z.; He, S.; Yuille, A.; Zhou, Y.; and Xie, C. 2022. A Simple Data Mixing Prior for Improving Self-Supervised Learning. In *CVPR*.

Riemer, M.; Cases, I.; Ajemian, R.; Liu, M.; Rish, I.; Tu, Y.; and Tesauro, G. 2019. Learning to learn without forgetting by maximizing transfer and minimizing interference. In *ICLR*.

Robins, A. V. 1995. Catastrophic Forgetting, Rehearsal and Pseudorehearsal. *Connect. Sci.*, 123–146.

Rusu, A. A.; Rabinowitz, N. C.; Desjardins, G.; Soyer, H.; Kirkpatrick, J.; Kavukcuoglu, K.; Pascanu, R.; and Hadsell, R. 2016. Progressive Neural Networks. arXiv:1606.04671.

Shen, Z.; Liu, Z.; Liu, Z.; Savvides, M.; Darrell, T.; and Xing, E. 2022. Un-Mix: Rethinking Image Mixtures for Unsupervised Visual Representation Learning. In *AAAI*.

Shoemake, K. 1985. Animating rotation with quaternion curves. *Proceedings of the 12th annual conference on Computer graphics and interactive techniques*.

Smith, J. S.; Karlinsky, L.; Gutta, V.; Cascante-Bonilla, P.; Kim, D.; Arbelle, A.; Panda, R.; Feris, R.; and Kira, Z. 2023. CODA-Prompt: COntinual Decomposed Attention-based Prompting for Rehearsal-Free Continual Learning. In *CVPR*.

Tang, C.; Qendro, L.; Spathis, D.; Kawsar, F.; Mascolo, C.; and Mathur, A. 2024. Kaizen: Practical self-supervised continual learning with continual fine-tuning. In *WACV*.

Thulasidasan, S.; Chennupati, G.; Bilmes, J.; Bhattacharya, T.; and Michalak, S. 2019. On Mixup Training: Improved Calibration and Predictive Uncertainty for Deep Neural Networks. In *NeurIPS*.

Tiwari, R.; Killamsetty, K.; Iyer, R.; and Shenoy, P. 2022. GCR: Gradient Coreset Based Replay Buffer Selection For Continual Learning. In *CVPR*.

Verma, V.; Lamb, A.; Beckham, C.; Najafi, A.; Mitliagkas, I.; Courville, A.; Lopez-Paz, D.; and Bengio, Y. 2019. Manifold Mixup: Better Representations by Interpolating Hidden States. In *ICML*.

Vitter, J. S. 1985. Random sampling with a reservoir. *ACM Transactions on Mathematical Software*, 37–57.

Wang, T.; and Isola, P. 2020. Understanding Contrastive Representation Learning through Alignment and Uniformity on the Hypersphere. In *ICML*.

Wang, Z.; Zhang, Z.; Ebrahimi, S.; Sun, R.; Zhang, H.; Lee, C.-Y.; Ren, X.; Su, G.; Perot, V.; Dy, J.; and Pfister, T. 2022a. DualPrompt: Complementary Prompting for Rehearsal-free Continual Learning. In *ECCV*.

Wang, Z.; Zhang, Z.; Lee, C.-Y.; Zhang, H.; Sun, R.; Ren, X.; Su, G.; Perot, V.; Dy, J.; and Pfister, T. 2022b. Learning to Prompt for Continual Learning. In *CVPR*.

Wen, Y.; Tan, Z.; Zheng, K.; Xie, C.; and Huang, W. 2024. Provable Contrastive Continual Learning. In *ICML*.

Yang, Y.; Chen, S.; Li, X.; Xie, L.; Lin, Z.; and Tao, D. 2022. Inducing Neural Collapse in Imbalanced Learning: Do We Really Need a Learnable Classifier at the End of Deep Neural Network? In *NeurIPS*.

Yang, Y.; Yuan, H.; Li, X.; Lin, Z.; Torr, P.; and Tao, D. 2023a. Neural Collapse Inspired Feature-Classifier Alignment for Few-Shot Class-Incremental Learning. In *ICLR*.

Yang, Y.; Yuan, H.; Li, X.; Wu, J.; Zhang, L.; Lin, Z.; Torr, P.; Tao, D.; and Ghanem, B. 2023b. Neural Collapse Terminus: A Unified Solution for Class Incremental Learning and Its Variants.

Yoon, J.; Yang, E.; Lee, J.; and Hwang, S. J. 2018. Lifelong Learning with Dynamically Expandable Networks. In *ICLR*.

Zbontar, J.; Jing, L.; Misra, I.; LeCun, Y.; and Deny, S. 2021. Barlow Twins: Self-Supervised Learning via Redundancy Reduction. In *ICML*.

Zenke, F.; Poole, B.; and Ganguli, S. 2017. Continual Learning Through Synaptic Intelligence. In *ICML*.

Zhang, H.; Cisse, M.; Dauphin, Y. N.; and Lopez-Paz, D. 2018. mixup: Beyond Empirical Risk Minimization. In *ICLR*.

Zhang, Y.; Hooi, B.; Hu, D.; Liang, J.; and Feng, J. 2021. Unleashing the Power of Contrastive Self-Supervised Visual Models via Contrast-Regularized Fine-Tuning. In *NeurIPS*.

Zhou, J.; Li, X.; Ding, T.; You, C.; Qu, Q.; and Zhu, Z. 2022. On the Optimization Landscape of Neural Collapse under MSE Loss: Global Optimality with Unconstrained Features. In *ICML*.

Zhu, Z.; Ding, T.; Zhou, J.; Li, X.; You, C.; Sulam, J.; and Qu, Q. 2021. A Geometric Analysis of Neural Collapse with Unconstrained Features. In *NeurIPS*.

A Theoretical Proof

In this section, we prove the theory that DR loss should be used instead of contrastive loss for mixed-up samples. Our proof uses the same technique as in (Yang et al. 2022), where they demonstrate that samples from minority class should not be learned with Cross-Entropy (CE) loss. However, in this work, we extend this proof in case of mixed-up samples when learning representation.

Contrastive loss. Specifically, these samples can not be learned with current supervised contrastive loss as SupCon (Khosla et al. 2020). Indeed, the equation of SupCon loss is as follows,

$$\mathcal{L}_{SupCon} = \sum_{i=1}^{2N} \frac{-1}{|P(i)|} \sum_{j \in P(i)} \log\left(\frac{e^{\langle \mathbf{x}_i \cdot \mathbf{z}_j \rangle / \tau}}{\sum_{k \in A(i)} e^{\langle \mathbf{x}_i \cdot \mathbf{z}_k \rangle / \tau}}\right) \quad (10)$$

where $\langle \cdot \rangle$ is the cosine similarity, $\tau > 0$ is the temperature factor, $A(i) = \{1..2N\} \setminus \{i\}$, and $P(i)$ is the index set of positive views with the anchor \mathbf{x}_i , denoted as:

$$P(i) = \{p \in \{1..2N\} | y_p = y_i, p \neq i\} \quad (11)$$

From equation of \mathcal{L}_{SupCon} , when using with mixed-up samples, since they have no positive views, $P(i) = \emptyset$ for all mixed-up samples. Therefore, \mathcal{L}_{SupCon} is always equal to 0. In the context of NC with fixed prototypes, recent loss functions like FNC² (Dang et al. 2025) (as described in Eq. (8)) can be used, but it is not efficient since it can break the optimal points. Similar to SupCon, when adapting \mathcal{L}_{FNC^2} for mixed-up samples, $P(i) = \emptyset$ for these samples. Therefore, this loss will become as follows (for simplify, we consider this loss for a specific mixed sample $\tilde{\mathbf{x}}$ with corresponding feature $\tilde{\mathbf{z}} = g^t(f^t(\tilde{\mathbf{x}}))$ and mixed prototype $\tilde{\mathbf{p}}$,

$$\mathcal{L}_{FNC^2}(\tilde{\mathbf{z}}) = -(1 - \tilde{r})^\gamma \log(\tilde{r}) \quad (12)$$

where

$$\tilde{r} = \frac{e^{\langle \tilde{\mathbf{z}} \cdot \tilde{\mathbf{p}} \rangle / \tau}}{\sum_{z_k \neq \tilde{\mathbf{z}}} e^{\langle \tilde{\mathbf{z}} \cdot \mathbf{z}_k \rangle / \tau} + \sum_{\mathbf{p}_l \in \mathbf{P}_{1:t-1}} e^{\langle \tilde{\mathbf{z}} \cdot \mathbf{p}_l \rangle / \tau}} \quad (13)$$

Since the focal term $(1 - \tilde{r})^\gamma$ is only used to encourage model focus more on hard samples which are far from their prototypes, we omit this term for simplicity and focus on the analysis:

$$\begin{aligned} \mathcal{L}_{FNC^2}(\tilde{\mathbf{z}}) &= -\log(\tilde{r}) \\ &= -\langle \tilde{\mathbf{z}} \cdot \tilde{\mathbf{p}} \rangle / \tau + \log(A) \end{aligned} \quad (14)$$

where $A = \sum_{z_k \neq \tilde{\mathbf{z}}} e^{\langle \tilde{\mathbf{z}} \cdot \mathbf{z}_k \rangle / \tau} + \sum_{\mathbf{p}_l \in \mathbf{P}_{1:t-1}} e^{\langle \tilde{\mathbf{z}} \cdot \mathbf{p}_l \rangle / \tau}$.

Here, the prototypes are fixed, only features are learnable, the gradient of \mathcal{L}_{FNC^2} for mixed-up samples with respect to $\tilde{\mathbf{z}}$ is:

$$\begin{aligned} \frac{\partial \mathcal{L}_{FNC^2}}{\partial \tilde{\mathbf{z}}} &= -\tilde{\mathbf{p}} / \tau + \frac{1}{A} \frac{\partial A}{\partial \tilde{\mathbf{z}}} \\ &= -\tilde{\mathbf{p}} / \tau + \sum_{z_k \neq \tilde{\mathbf{z}}} (\mathbf{z}_k / \tau) \frac{e^{\langle \tilde{\mathbf{z}} \cdot \mathbf{z}_k \rangle / \tau}}{A} \\ &\quad + (\mathbf{p}_l / \tau) \sum_{\mathbf{p}_l \in \mathbf{P}_{1:t-1}} \frac{e^{\langle \tilde{\mathbf{z}} \cdot \mathbf{p}_l \rangle / \tau}}{A} \\ &= -\tilde{\mathbf{p}} / \tau + \sum_{z_k \neq \tilde{\mathbf{z}}} (\mathbf{z}_k / \tau) \mathcal{F}(\mathbf{z}_k) \\ &\quad + \sum_{\mathbf{p}_l \in \mathbf{P}_{1:t-1}} (\mathbf{p}_l / \tau) \mathcal{F}(\mathbf{p}_l) \end{aligned} \quad (15)$$

with $\mathcal{F}(a) = \frac{e^{\langle \tilde{\mathbf{z}} \cdot a \rangle / \tau}}{A}$. The negative gradient $-\frac{\partial \mathcal{L}_{FNC^2}}{\partial \tilde{\mathbf{z}}}$ can be decoupled as the combination of pulling and pushing term:

$$\mathbf{G}_{pull} = -\tilde{\mathbf{p}} / \tau$$

$$\mathbf{G}_{push} = \sum_{z_k \neq \tilde{\mathbf{z}}} (\mathbf{z}_k / \tau) \mathcal{F}(\mathbf{z}_k) + \sum_{\mathbf{p}_l \in \mathbf{P}_{1:t-1}} (\mathbf{p}_l / \tau) \mathcal{F}(\mathbf{p}_l) \quad (16)$$

The pulling term \mathbf{G}_{pull} pulls the mixed-up sample $\tilde{\mathbf{z}}$ towards its mixed prototype $\tilde{\mathbf{p}}$, while the pushing term \mathbf{G}_{push} pushes $\tilde{\mathbf{z}}$ away from the other samples features ($\forall \mathbf{z}_k \neq \tilde{\mathbf{z}}$) and previous prototypes $\mathbf{P}_{1:t-1}$.

The “push” gradient \mathbf{G}_{push} is crucial for learning classifiers. However, here, $\tilde{\mathbf{p}}$ is not learnable as it is created by mixing fixed prototypes; therefore, the “push” term is unnecessary and can even cause deviation since it does not direct to the corresponding mixed prototype as the “pull” term does. Furthermore, it can be observed that \mathbf{G}_{pull} is dominated by \mathbf{G}_{push} , making it difficult to converge and inducing a mixed-up configuration (Fisher, Meng, and Popyan 2024). Building on these insights, we opt not to use contrastive loss such as \mathcal{L}_{FNC^2} for mixed-up samples.

Dot-Regression loss. The gradient of the Dot-Regression (DR) loss is provided in (Yang et al. 2022), with a mixed-up sample $\tilde{\mathbf{x}}$ and corresponding feature $\tilde{\mathbf{z}}$, it is calculated as follows,

$$\frac{\partial \mathcal{L}_{DR}}{\partial \tilde{\mathbf{z}}} = -(1 - \langle \tilde{\mathbf{z}} \cdot \tilde{\mathbf{p}} \rangle) \tilde{\mathbf{p}} \quad (17)$$

This gradient matches the first term in Eq. (15), which functions as a “pull”, but it has no “push” term. Since it only pulls the mixed sample towards the corresponding mixed prototype, which is not learnable, it helps to accelerate learning without encountering the issues associated with FNC². Therefore, in this work, we choose the DR loss for learning from mixed samples.

B Neural Collapse Concept

The concept of NC is defined as follows.

Definition 1. A simplex Equiangular Tight Frame (ETF) consists of a set of K vectors: $\mathbf{Q} = \{\mathbf{q}_k\}_{k=1}^K$, each vector $\mathbf{q}_k \in \mathbb{R}^d$, $K \leq d + 1$, which satisfies:

$$\mathbf{Q} = \sqrt{\frac{K}{K-1}} \mathbf{U} \left(\mathbf{I}_K - \frac{1}{K} \mathbf{1}_K \mathbf{1}_K^T \right), \quad (18)$$

where $\mathbf{U} \in \mathbb{R}^{d \times K}$ is an orthogonal basis and $\mathbf{U}^T \mathbf{U} = \mathbf{I}_K$, \mathbf{I}_K is an identity matrix and $\mathbf{1}_K$ is an all-ones vector.

Every vector \mathbf{q}_k has the same ℓ_2 norm, and the inner product between any pair of distinct vectors is given by $-\frac{1}{K-1}$, which represents the lowest possible cosine similarity for K equiangular vectors in \mathbb{R}^d . This configuration can be expressed as follows:

$$\mathbf{q}_i^T \mathbf{q}_j = \frac{K}{K-1} \delta_{i,j} - \frac{1}{K-1}, \quad \forall i, j \in [1, K], \quad (19)$$

where $\delta_{i,j} = 1$ in case of $i = j$, and 0 otherwise.

Subsequently, the NC phenomenon can be formally characterized by the following four attributes (Papyan, Han, and Donoho 2020):

NC1: The features from the final layer corresponding to the same class converge to their intra-class mean, ensuring that the covariance approaches zero, i.e., $\Sigma_V^k \rightarrow \mathbf{0}$. Mathematically, this is expressed as: $\Sigma_V^k = \text{Avg}_i \{(\boldsymbol{\nu}_{k,i} - \boldsymbol{\mu}_k)(\boldsymbol{\nu}_{k,i} - \boldsymbol{\mu}_k)^T\}$, where $\boldsymbol{\nu}_{k,i}$ is the feature of sample i in class k , and $\boldsymbol{\mu}_k$ denotes the intra-class feature mean.

NC2: When centered by the global mean, intra-class means align with the vertices of a simplex ETF. That is, the set $\{\tilde{\boldsymbol{\mu}}_k\}$, $1 \leq k \leq K$ satisfy Eq. (19), where $\tilde{\boldsymbol{\mu}}_k = \frac{(\boldsymbol{\mu}_k - \boldsymbol{\mu}_G)}{\|\boldsymbol{\mu}_k - \boldsymbol{\mu}_G\|}$ and global mean $\boldsymbol{\mu}_G = \frac{1}{K} \sum_{k=1}^K \boldsymbol{\mu}_k$;

NC3: The intra-class means, after centering by the global mean, align with their respective classifier weight vectors, forming the same simplex ETF. This relationship is given by $\tilde{\boldsymbol{\mu}}_k = \frac{\mathbf{w}_k}{\|\mathbf{w}_k\|}$, where $1 \leq k \leq K$ and \mathbf{w}_k is the classifier weight of class k ;

NC4: When NC1-NC3 are satisfied, model predictions simplify to selecting class center closest to the feature representation. This is represented as $\text{argmax}_k \langle \mathbf{z}, \mathbf{w}_k \rangle = \text{argmin}_k \|\mathbf{z} - \boldsymbol{\mu}_k\|$, where $\langle \cdot, \cdot \rangle$ denotes the inner product operator, and \mathbf{z} is the model's output feature.

C Definitions of Distillation Losses

In stability learning, we use hardness-softness distillation (HSD) due to its effectiveness compared to instance-wise relation distillation (IRD) and sample-prototype relation distillation (S-PRD). The definition of HSD is as follows,

$$\mathcal{L}_{HSD} = (1 - \xi) \mathcal{L}_{IRD} + \xi \mathcal{L}_{S-PRD} \quad (20)$$

where $\xi = \max(0, \frac{e - e_0}{E})$, e represents the epoch index, e_0 denotes the number of epochs used for the warm-up period, and E is the total number of epochs.

$$\begin{cases} \mathcal{L}_{IRD} = \sum_{i=1}^{2N} -\mathbf{o}^{t-1}(\mathbf{x}_i) \cdot \log(\mathbf{o}^t(\mathbf{x}_i)) \\ \mathcal{L}_{S-PRD} = \sum_{i=1}^{2N} -\mathbf{q}^{t-1}(\mathbf{x}_i; \mathbf{P}_{1:t}) \cdot \log(\mathbf{q}^t(\mathbf{x}_i; \mathbf{P}_{1:t})) \end{cases} \quad (21)$$

In the loss \mathcal{L}_{IRD} (Cha, Lee, and Shin 2021), $\mathbf{o}^t(\mathbf{x}_i)$ is defined as:

$$\mathbf{o}^t(\mathbf{x}_i) = [o_{i,1}^t, \dots, o_{i,i-1}^t, o_i^t, o_{i,i+1}^t, \dots, o_{i,2N}^t] \quad (22)$$

Each individual element $o_{i,1}^t$ is computed as:

$$o_{i,j}^t = \frac{e^{\langle \mathbf{z}_i^t \cdot \mathbf{z}_j^t \rangle / \kappa}}{\sum_{k \neq i} e^{\langle \mathbf{z}_i^t \cdot \mathbf{z}_k^t \rangle / \kappa}} \quad (23)$$

where κ is the temperature hyperparameter, and $t \geq 1$ is the task index. For the loss \mathcal{L}_{S-PRD} (Dang et al. 2025), given the prototype set $\mathbf{P}_{1:t} = \{\mathbf{p}_s\}_{s=1}^S$, which includes all prototypes used from task 1 to task t . The definition of \mathcal{L}_{S-PRD} is defined as,

$$\mathbf{q}^t(\mathbf{x}_i; \mathbf{P}_{1:t}) = [q_{i,1}^t, q_{i,2}^t, \dots, q_{i,S}^t] \quad (24)$$

where each $q_{i,j}^t$ is computed as:

$$q_{i,j}^t = \frac{e^{\langle \mathbf{z}_i^t \cdot \mathbf{p}_j \rangle / \zeta}}{\sum_{s=1}^S e^{\langle \mathbf{z}_i^t \cdot \mathbf{p}_s \rangle / \zeta}} \quad (25)$$

with ζ being the temperature factor.

D Additional Training Details

D.1 Data Preparation

Similar to other baselines (Cha, Lee, and Shin 2021; Dang et al. 2025; Wen et al. 2024), we apply a standard set of augmentations in the CL literature for each image as follows (using Pytorch (Paszke et al. 2019) notations):

- **RandomResizedCrop**. We apply random cropping with scales of $[0.2, 1.0]$, $[0.2, 1.0]$, $[0.1, 1.0]$ for Seq-Cifar-10, Seq-Cifar-100, and Seq-Tiny-ImageNet, respectively, and resize the images to 32×32 , 32×32 , and 64×64 .
- **RandomHorizontalFlip**. We horizontally flip each image with a probability of 0.5.
- **ColorJitter**. We adjust brightness, contrast, saturation, and hue with maximum strengths of 0.4, 0.4, 0.4, and 0.1, respectively, with probability 0.8.
- **RandomGrayscale**. We convert images to grayscale with a probability of 0.2 to increase appearance invariance.
- **GaussianBlur**. For Seq-Tiny-ImageNet, Gaussian blur is applied with a 7×7 kernel and a standard deviation randomly sampled from $[0.1, 2.0]$, with a probability of 0.5.

In addition, following (Buzzega et al. 2020; Cha, Lee, and Shin 2021; Dang et al. 2025; Wen et al. 2024), each batch is sampled equally and independently from the union of current task data and memory, eliminating the need to control old samples, avoiding sample imbalances and single-class batches that can degrade contrastive loss like FNC² (Dang et al. 2025).

D.2 Algorithm Overview

The overview of our method is summarized in Algorithm 1.

D.3 Hyperparameter Selection

We utilize a grid search method to select the optimal hyperparameters, using a randomly drawn 10% of the training data as the validation set.

Baseline. The baseline hyperparameters under evaluation include:

- Number of initial epochs (E_1)

Hyperparameter	Values
E_1	{500}
$E_{t \geq 2}$	{50, 100}
η	{0.1, 0.5, 1.0}
bsz	{256, 512}
γ	{0, 1, 2, 4, 7, 10}
τ	{0.1, 0.5, 1.0}
κ_{past}	{0.01, 0.05, 0.1}
$\kappa_{current}$	{0.1, 0.2}
ζ_{past}	{0.01, 0.05, 0.1}
$\zeta_{current}$	{0.1, 0.2}
e_0	{10, 20, 30}
α	{1, 10, 25}
M	{5, 10, 15}
v	{1, 2, 5, 10}
ι	{1, 2, 5, 10}

Table 3: Search spaces of all hyperparameters. Baselines use the top set; while SAMix tunes **only 4** additional hyperparameters below.

- Number of epochs of t -th task ($E_{t \geq 2}$)
- Learning rate (η)
- Batch size (bsz)
- Focusing hyperparameters (γ) for FNC² loss
- Temperature for the Focal Neural Collapse Contrastive (FNC²) (τ)
- Temperature for instance-wise relation distillation loss (\mathcal{L}_{IRD}): Following (Cha, Lee, and Shin 2021), we employ distinct temperature hyperparameters for the similarity vectors of past (κ_{past}) and current ($\kappa_{current}$) data
- Temperature for sample-prototype relation distillation loss (\mathcal{L}_{S-PRD}): We use different temperature hyperparameters, ζ_{past} for past similarity vectors and $\zeta_{current}$ for current similarity vectors
- Number of warm-up epochs in hardness-softness distillation loss (\mathcal{L}_{HSD}) (e_0)

These baseline hyperparameters are **tuned once** for the baselines *without SAMix* and **kept fixed** when integrating *SAMix*.

When using SAMix. In addition to these tuned baseline values, we further tune only four hyperparameters: M , α , v , and ι , listed as:

- Hyperparameter (α) of the Beta(α, α) to control the mixing coefficient λ in SAMix
- Number of bins (M) to compute the expected calibration error
- Balancing hyperparameters v and ι for learning mixed samples in the DR-based and FNC²-based plasticity methods, respectively

The search space for all hyperparameters is listed in Table 3. The final chosen values for the baselines and SAMix-integrated methods are detailed in Table 4 and Table 5, respectively. When **using SAMix**, we select $M = 15$, $\alpha = 25$

Algorithm 1: *Sphere-Adaptive Mixup (SAMix) in Neural Collapse-based Continual Learning*

```

1: Input: Training sets  $\{\mathcal{D}_t\}_{t=1}^T$ , backbone  $f$ , projector  $g$ , predictor  $h$ , fixed prototypes  $\mathbf{P}$ , hyperparameters  $v, \iota, \alpha$ , learning rate  $\eta$ , plasticity loss type ploss_type
2: Initialize model  $(g \circ f)_{\theta}$  and buffer  $\mathcal{M} \leftarrow \emptyset$ ,
3: for  $t = 1, \dots, T$  do
4:   for batch  $\mathcal{B}_t \sim \mathcal{D}_t \cup \mathcal{M}$  do
5:      $\lambda \leftarrow \text{Beta}(\alpha, \alpha)$ 
6:      $\mathcal{B}_{mix} \leftarrow \text{SAMix}(\mathcal{B}_t, \lambda)$  with Eq. (1)
7:      $\mathbf{P}_{mix} \leftarrow \text{SAMix}(\mathbf{P}, \lambda)$  with Eq. (6)
8:     if ploss_type is DR then
9:        $\mathcal{L} \leftarrow \mathcal{L}_{DR}(\theta; \mathcal{B}_t) + v\mathcal{L}_{DR}(\theta; \mathcal{B}_{mix})$ 
10:    else
11:       $\mathcal{L} \leftarrow \mathcal{L}_{FNC^2}(\theta; \mathcal{B}_t) + \iota\mathcal{L}_{DR}(\theta; \mathcal{B}_{mix})$ 
12:    end if
13:    if  $t > 1$  then
14:       $\mathcal{L} \leftarrow \mathcal{L} + \mathcal{L}_{HSD}(\theta; \theta_{prev}, \mathcal{B}_t)$ 
15:    end if
16:     $\theta \leftarrow \theta - \eta \nabla_{\theta} \mathcal{L}$ 
17:  end for
18:   $\mathcal{M} \leftarrow \text{Reservoir}(\mathcal{M} \cup \mathcal{D}_t)$ 
19:   $\theta_{prev} \leftarrow \theta$ 
20: end for

```

for all scenarios, and $v = \iota = 5$ for both the FC-NCCL and TA-NCCL methods. To maintain focus, we exclude hyperparameters previously discovered in the literature.

D.4 Training Schedules

In training. For all experiments, we choose SGD as the optimizer with momentum of 0.9 and weight decay of 0.0001. The learning rate is warmed up for 10 epochs and then decayed using the cosine schedule (Loshchilov and Hutter 2017), which restarts at the beginning of each new task.

In evaluation. A linear classifier is trained for 100 epochs using SGD with momentum 0.9 and no weight decay. The initial learning rates are 1.0, 0.1, 0.1 for Seq-Cifar-10, Seq-Cifar-100, Seq-Tiny-ImageNet, respectively, then decayed exponentially by a factor of 0.2 at epochs 60, 75, and 90.

E Additional Results

E.1 Average forgetting results

The Average Forgetting metric (Chaudhry et al. 2018), used in this work to quantify model forgetting, is defined as:

$$F = \frac{1}{T-1} \sum_{i=1}^{T-1} \max_{t \in \{1, \dots, T-1\}} (A_{t,i} - A_{T,i}) \quad (26)$$

Table 6 reports the average forgetting results of our method compared to all other baselines. The results demonstrate that our method effectively mitigates forgetting, even without relying on additional buffers.

E.2 Calibration Error and Overconfidence

Table 7 shows the changes Average Expected Calibration Error (AECE) and Average Overconfidence Error (AOE),

Method	Buffer size	Dataset	Hyperparameter
FC-NCCL	0, 200, 500	Seq-Cifar-10	$bsz: 512, \eta: 0.5, \gamma: 1, E_1: 500, E_{t \geq 2}: 100,$ $\tau: 0.5, e_0: 30, \kappa_{past}: 0.01, \kappa_{current}: 0.2,$ $\zeta_{past}: 0.01, \zeta_{current}: 0.2$
		Seq-Cifar-100	$bsz: 512, \eta: 0.5, \gamma: 4, E_1: 500, E_{t \geq 2}: 100,$ $\tau: 0.5, e_0: 30, \kappa_{past}: 0.01, \kappa_{current}: 0.2,$ $\zeta_{past}: 0.1, \zeta_{current}: 0.2$
	0, 200, 500	Seq-Tiny-ImageNet	$bsz: 512, \eta: 0.1, \gamma: 4, E_1: 500, E_{t \geq 2}: 50,$ $\tau: 0.5, e_0: 20, \kappa_{past}: 0.1, \kappa_{current}: 0.1,$ $\zeta_{past}: 0.1, \zeta_{current}: 0.2$
TA-NCCL	0, 200, 500	Seq-Cifar-10	$bsz: 512, \eta: 0.5, E_1: 500, E_{t \geq 2}: 100,$ $\tau: 0.5, e_0: 30, \kappa_{past}: 0.01, \kappa_{current}: 0.2,$ $\zeta_{past}: 0.01, \zeta_{current}: 0.2$
		Seq-Cifar-100	$bsz: 512, \eta: 0.5, E_1: 500, E_{t \geq 2}: 100,$ $\tau: 0.5, e_0: 30, \kappa_{past}: 0.01, \kappa_{current}: 0.2,$ $\zeta_{past}: 0.1, \zeta_{current}: 0.2$
	0, 200, 500	Seq-Tiny-ImageNet	$bsz: 512, \eta: 0.1, E_1: 500, E_{t \geq 2}: 50,$ $\tau: 0.5, e_0: 20, \kappa_{past}: 0.1, \kappa_{current}: 0.1,$ $\zeta_{past}: 0.1, \zeta_{current}: 0.2$

Table 4: Selected baseline hyperparameters in our experiments.

Method	Buffer size	Dataset	Hyperparameter
FC-NCCL + SAMix	0, 200, 500	Seq-Cifar-10	$bsz: 512, \eta: 0.5, \gamma: 1, E_1: 500, E_{t \geq 2}: 100,$ $\tau: 0.5, e_0: 30, \kappa_{past}: 0.01, \kappa_{current}: 0.2,$ $\zeta_{past}: 0.01, \zeta_{current}: 0.2,$ $M : 15, \alpha : 25, v : 5, \iota : 5$
		Seq-Cifar-100	$bsz: 512, \eta: 0.5, \gamma: 4, E_1: 500, E_{t \geq 2}: 100,$ $\tau: 0.5, e_0: 30, \kappa_{past}: 0.01, \kappa_{current}: 0.2,$ $\zeta_{past}: 0.1, \zeta_{current}: 0.2,$ $M : 15, \alpha : 25, v : 5, \iota : 5$
	0, 200, 500	Seq-Tiny-ImageNet	$bsz: 512, \eta: 0.1, \gamma: 4, E_1: 500, E_{t \geq 2}: 50,$ $\tau: 0.5, e_0: 20, \kappa_{past}: 0.1, \kappa_{current}: 0.1,$ $\zeta_{past}: 0.1, \zeta_{current}: 0.2,$ $M : 15, \alpha : 25, v : 5, \iota : 5$
TA-NCCL + SAMix	0, 200, 500	Seq-Cifar-10	$bsz: 512, \eta: 0.5, E_1: 500, E_{t \geq 2}: 100,$ $\tau: 0.5, e_0: 30, \kappa_{past}: 0.01, \kappa_{current}: 0.2,$ $\zeta_{past}: 0.01, \zeta_{current}: 0.2,$ $M : 15, \alpha : 25, v : 5, \iota : 5$
		Seq-Cifar-100	$bsz: 512, \eta: 0.5, E_1: 500, E_{t \geq 2}: 100,$ $\tau: 0.5, e_0: 30, \kappa_{past}: 0.01, \kappa_{current}: 0.2,$ $\zeta_{past}: 0.1, \zeta_{current}: 0.2,$ $M : 15, \alpha : 25, v : 5, \iota : 5$
	0, 200, 500	Seq-Tiny-ImageNet	$bsz: 512, \eta: 0.1, E_1: 500, E_{t \geq 2}: 50,$ $\tau: 0.5, e_0: 20, \kappa_{past}: 0.1, \kappa_{current}: 0.1,$ $\zeta_{past}: 0.1, \zeta_{current}: 0.2,$ $M : 15, \alpha : 25, v : 5, \iota : 5$

Table 5: Selected hyperparameters when integrating SAMix. Differences from the baselines are shown in bold, **only 4** additional hyperparameters are tuned.

Buffer	Dataset Scenario	Venue	Seq-Cifar-100		Seq-Tiny-ImageNet		Seq-Cifar-10	
			Class-IL	Task-IL	Class-IL	Task-IL	Class-IL	Task-IL
0	Co ² L(Cha, Lee, and Shin 2021)	ICCV'21	66.51±0.28	39.63±0.62	62.80±0.77	39.54±1.08	35.81±1.08	14.33±0.87
	FC-NCCL (Dang et al. 2025)	WACV'25	52.03±0.63	36.20±0.48	53.97±0.63	37.57±0.88	23.85±0.30	4.72±0.28
	FC-NCCL (Dang et al. 2025)(+ SAMix)		44.30±0.59	26.54±0.88	52.39±0.75	37.16±0.53	27.45±1.49	7.47±1.22
	Ours		44.69±0.67	19.07±0.73	41.38±0.89	27.99±0.76	22.20±0.79	2.05±0.18
	Ours(+ SAMix)		42.53±0.97	20.69±0.75	51.61±0.55	36.53±0.62	21.47±0.68	2.01±0.29
200	ER (Riemer et al. 2019)	ICLR'19	75.06±0.63	27.38±1.46	76.53±0.51	40.47±1.54	59.30±2.48	6.07±1.09
	DER(Buzzega et al. 2020)	NeurIPS'20	62.72±2.69	25.98±1.55	64.83±1.48	40.43±1.05	35.79±2.59	6.08±0.70
	Co ² L (Cha, Lee, and Shin 2021)	ICCV'21	67.82±0.41	38.22±0.34	73.25±0.21	47.11±1.04	36.35±1.16	6.71±0.35
	GCR(Tiwari et al. 2022)	CVPR'22	57.65±2.48	24.12±1.17	65.29±1.73	40.36±1.08	32.75±2.67	7.38±1.02
	CILA(Wen et al. 2024)	ICML'24	-	-	-	-	-	-
	CCLIS(Li et al. 2024a)	AAAI'24	46.89±0.59	14.17±0.20	62.21±0.34	33.20±0.75	22.59±0.18	2.08±0.27
	FC-NCCL (Dang et al. 2025)	WACV'25	52.40±0.83	33.66±0.24	52.07±0.46	33.76±0.58	25.24±0.69	4.28±0.32
	FC-NCCL (Dang et al. 2025)(+ SAMix)		42.83±0.17	25.29±1.03	50.37±0.33	32.77±0.46	26.64±0.88	4.34±0.25
500	Ours		42.40±0.43	13.59±1.51	42.22±0.44	27.85±0.58	20.89±1.05	1.84±0.30
	Ours(+ SAMix)		39.24±1.26	16.51±0.53	51.66±0.75	30.89±0.53	20.54±0.44	1.27±0.21
	ER (Riemer et al. 2019)	ICLR'19	67.96±0.78	17.37±1.06	75.21±0.54	30.73±0.62	43.22±2.10	3.50±0.53
	DER(Buzzega et al. 2020)	NeurIPS'20	49.07±2.54	25.98±1.55	59.95±2.31	28.21±0.97	24.02±1.63	3.72±0.55
	Co ² L (Cha, Lee, and Shin 2021)	ICCV'21	51.23±0.65	26.30±0.57	65.15±0.26	39.22±0.69	25.33±0.99	3.41±0.80
500	GCR(Tiwari et al. 2022)	CVPR'22	39.20±2.84	15.07±1.88	56.40±1.08	27.88±1.19	19.27±1.48	3.14±0.36
	CILA(Wen et al. 2024)	ICML'24	-	-	-	-	-	-
	CCLIS(Li et al. 2024a)	AAAI'24	42.53±0.64	12.68±1.33	50.15±0.20	23.46±0.93	18.93±0.61	1.69±0.12
	FC-NCCL (Dang et al. 2025)	WACV'25	41.66±0.78	24.84±0.91	46.08±0.56	26.45±0.79	22.59±1.02	3.21±0.25
	FC-NCCL (Dang et al. 2025)(+ SAMix)		34.23±0.14	17.26±0.80	45.14±0.76	25.31±0.84	20.07±0.72	3.94±0.25
500	Ours		31.38±1.48	9.66±0.79	35.62±0.62	21.51±0.93	16.85±0.43	1.39±0.20
	Ours(+ SAMix)		29.94±1.06	9.98±0.91	43.53±0.59	22.87±0.61	15.25±0.53	1.16±0.12

Table 6: Average forgetting (lower is better) across 5 independent trials from 5 different seeds: Comparing our method against all baselines in continual learning. **(Ours: TA-NCCL method)**

Buffer	Dataset Scenario	Seq-Cifar-100			Seq-Tiny-ImageNet			Seq-Cifar-10		
		AECE(↓)	AOE(↓)	$A_{T,T}(\uparrow)$	AECE(↓)	AOE(↓)	$A_{T,T}(\uparrow)$	AECE(↓)	AOE(↓)	$A_{T,T}(\uparrow)$
0	FC-NCCL (Dang et al. 2025)	0.160	0.107	74.25	0.130	0.050	69.70	0.206	0.167	88.30
	FC-NCCL (Dang et al. 2025)(+ SAMix)	0.141 ▲	0.082 ▲	77.00 ▲	0.088 ▲	0.021 ▲	74.40 ▲	0.177 ▲	0.133 ▲	85.60 ▽
	Ours	0.133	0.029	46.60	0.258	0.117	57.10	0.098	0.055	80.20
	Ours(+ SAMix)	0.106 ▲	0.005 ▲	78.55 ▲	0.146 ▲	0.069 ▲	63.30 ▲	0.152 ▽	0.099 ▽	85.15 ▲
200	FC-NCCL (Dang et al. 2025)	0.162	0.109	73.85	0.170	0.073	69.70	0.305	0.252	95.70
	FC-NCCL (Dang et al. 2025)(+ SAMix)	0.139 ▲	0.046 ▲	77.30 ▲	0.095 ▲	0.033 ▲	73.40 ▲	0.312 ▽	0.273 ▽	89.30 ▽
	Ours	0.140	0.035	53.80	0.251	0.112	59.20	0.153	0.108	84.40
	Ours(+ SAMix)	0.098 ▲	0.017 ▲	80.15 ▲	0.146 ▲	0.069 ▲	64.70 ▲	0.219 ▽	0.172 ▽	91.25 ▲
500	FC-NCCL (Dang et al. 2025)	0.231	0.164	71.95	0.098	0.040	63.20	0.334	0.290	96.40
	FC-NCCL (Dang et al. 2025)(+ SAMix)	0.132 ▲	0.092 ▲	76.50 ▲	0.079 ▲	0.031 ▲	64.20 ▲	0.267 ▲	0.226 ▲	93.60 ▽
	Ours	0.098	0.036	51.15	0.206	0.095	48.00	0.086	0.056	83.55
	Ours(+ SAMix)	0.078 ▲	0.015 ▲	80.05 ▲	0.115 ▲	0.052 ▲	56.80 ▲	0.150 ▽	0.122 ▽	92.55 ▲

Table 7: AECE, AOE, and last task accuracy ($A_{T,T}$) across different NC-based methods. **▲/▽** indicate methods applying SAMix outperforms/underperforms compared to methods without SAMix. All results indicate that SAMix is highly effective on large, complex datasets such as Seq-Cifar-100 and Seq-Tiny-ImageNet but largely ineffective on smaller datasets like Seq-Cifar-10.

and accuracy on the last task ($A_{T,T}$) when learning using SAMix. As can be seen from this table, NC-based methods using SAMix improve calibration and reduce overconfidence while maintaining superior performance compared to their original counterparts on complex datasets such as Seq-Cifar-10 and Seq-Tiny-ImageNet. However, on the smaller dataset Seq-Cifar-10, SAMix exhibits the opposite trend, aligning with the performance variations across tasks, as shown in Table 1.

E.3 Additional Ablation Studies

Extra time when using SAMix.

Although our method increase batch size (see Sec. 3.4), mixed samples are used only in the plasticity loss (DR), not in distillation or contrastive losses like FNC² to avoid disrupting the mixed-up configuration (see Appendix proof). Thus, mixed samples are not used as regular inputs, keeping

the impact on training time minimal. Table 8 shows the extra time when applying SAMix to FC-NCCL and TA-NCCL on Seq-Cifar-100 (CIL setting). Across buffer sizes, the additional time is a good trade-off, justified by significant performance gains. As in the discussion of (Chen et al. 2025), other SOTA CL methods such as L2P (Wang et al. 2022b) and DualPrompt (Wang et al. 2022a) increase training time by 37% and 32%, respectively, for performance gains of only 2.5% and 1.4%.

Performance with reduced batch size.

To evaluate SAMix under smaller batches, we run TA-NCCL on Seq-Cifar-10 (Class-IL setting) with a batch size of 256 with different buffer sizes. As shown in Table 9, even **without** memory, SAMix with half the batch size outperforms the SOTA method CCLIS (Li et al. 2024a), which uses a batch size of 512 and memory size of 200. This highlights

the strong adaptability of our method under constrained settings.

Buffer	0		200		500	
	Overhead	Gain	Overhead	Gain	Overhead	Gain
FC-NCCL	14.1	7.6	16.5	7.9	19.8	7.6
TA-NCCL	22.3	10.9	21.7	10.2	28.1	14.1

Table 8: Extra time (overhead) and performance gain (%) *with SAMix* on Seq-Cifar-100 (CIL setting).

Buffer	Method	Batch size	AA
0	TA-NCCL	512	44.41
	TA-NCCL	256	42.77
200	CCLIS	512	42.39
	TA-NCCL	512	46.95
	TA-NCCL	256	45.21

Table 9: SAMix results with varying batch sizes on Seq-Cifar-100 (CIL setting). Bold indicates comparison purposes.